

Rotating Convection and Gravito-Inertial Wave Generation in Stellar Interiors

K. C. Augustson¹, S. Mathis¹

¹AIM, CEA, CNRS, Université Paris-Saclay, Université Paris Diderot, Sorbonne Paris Cité, F-91191 Gif-sur-Yvette Cedex, France

Abstract

Gravito-inertial waves can be excited at the interface of convective and radiative regions and by the Reynolds stresses in the bulk of the convection zone. The magnitude of their energy flux will therefore vary with the properties of the convection. To assess how convection changes with rotation, a simplified local monomodal model for rotating convection is presented that provides the magnitude of the rms velocity, degree of superadiabaticity, and characteristic length scale as a function of the convective Rossby number as well as with thermal and viscous diffusivities. In the context of this convection model, two models for assessing the gravito-inertial wave flux are considered: an interfacial model and a full treatment of the Reynolds stress impact on the waves. It is found that there are regimes where the sub-inertial waves may carry a significant energy flux relative to pure gravity waves that depend upon the convective Rossby number, the ratio of the buoyancy time-scale in the stable region to the convective overturning time, and the wave frequency.

1 Introduction

Convection in stars is driven through buoyancy and doubly-diffusive instabilities, where it primarily serves to transport the energy released deep within the star or planet through regions where radiative energy transport is inefficient. Moreover, convection directly and nonlocally transports heat and chemicals through advection, entrainment, and dissipative processes (e.g., Miesch & Toomre, 2009; Kupka & Muthsam, 2017; Garaud, 2018). In the presence of rotation, convection can also transport angular momentum through Reynolds stresses and meridional flows to establish and maintain a differential rotation (e.g., Glatzmaier & Gilman, 1982; Kichatinov, 1986; Brun & Toomre, 2002; Miesch & Toomre, 2009). Convective motions that penetrate into subadiabatic regions also generate waves that propagate in the otherwise quiescent regions, providing another means for transport and mixing in those regions (e.g., Zahn *et al.*, 1997; Kumar *et al.*, 1999; Mathis, 2009). Gravito-inertial waves can be generated both near the transition between convectively stable and unstable regions and throughout the convection zone itself, while they propagate into the radiation zone (e.g., Press, 1981; Rogers *et al.*, 2013; Lecoanet *et al.*, 2015). They therefore transport angular momentum and chemical species, which are deposited where these waves are dissipated either through thermal diffusion, nonlinear wave breaking (e.g., Rogers, 2015; Rogers & McElwaine, 2017), or at critical layers (Alvan *et al.*, 2013; Jouve & Ogilvie, 2014). Such waves have been identified through asteroseismology as one of the candidates to explain angular momentum transport within stellar radiation zones across the entire Hertzsprung-Russell diagram (e.g., Garcia *et al.*, 2007; Saio *et al.*, 2015; Aerts *et al.*, 2017). Indeed, it has been demonstrated that for the Sun, evolved low-mass stars, and early-type stars stochastically excited internal gravity waves can lead to an efficient transport of angular momentum (e.g., Talon & Charbonnel, 2005; Mathis, 2013; Pinçon *et al.*, 2017). When rotation are present, gravito-inertial waves (e.g., Dintrans *et al.*, 1999; Dintrans & Rieutord, 2000; Davidson, 2013), as well as new instabilities, can be excited. They can lead to other channels of global-scale transport phenomena, some of which can become important through the coupling of inertial waves to convection throughout the convectively unstable zone (e.g.,

Mathis, 2013; Mathis *et al.*, 2014; Fuller *et al.*, 2015; Stello *et al.*, 2016; Lecoanet *et al.*, 2017). Therefore, the impact of rotation on both the driving mechanism of internal waves in stars and the transport induced by those waves needs to be understood and clarified.

In this work, a generalized version of a heuristic model for convection for rotating systems is presented following Stevenson (1979), Barker *et al.* (2014), and Augustson & Mathis (2018). This model of convection is then employed to estimate the gravito-inertial wave flux into the stable region adjacent to the convective region. Following the arguments of Press (1981) and André *et al.* (2017), the interfacial generation of gravito-inertial waves and their associated energy flux is assessed with respect to this convection model in §4. Subsequently, an estimate is given for the gravito-inertial wave flux for waves excited by Reynolds stresses using the wave amplitudes derived in Mathis *et al.* (2014) and the turbulence model constructed here and in Lecoanet & Quataert (2013). A summary of the results and perspectives are presented in §5.

2 General Framework

The heuristic model will be considered to be local such that the length scales of the flow are much smaller than either density or pressure scale heights. This is equivalent to ignoring the global dynamics and assuming that the convection can be approximated as local at each radius and colatitude in a star or planet. As such, one may consider the dynamics to be Boussinesq. In other words, the model consists of an infinite Cartesian plane of a nearly incompressible fluid with a small thermal expansion coefficient $\alpha_T = -\partial \ln \rho / \partial T|_P$ that is confined between two impenetrable plates differing in temperature by ΔT and separated by a distance ℓ_0 . As seen in many papers regarding Boussinesq dynamics (e.g., Chandrasekhar, 1961), the linearized Boussinesq equations can be reduced to a single third-order in time and eighth-order in space equation for the vertical velocity. The difference here, and in the work of Stevenson (1979), is that the state that the system is being linearized about is nonlinearly saturated, meaning that the potential temperature gradient is given by the Malkus-Howard convection theory (e.g., Malkus, 1954;

Howard, 1963). Together, these equations provide a dispersion relationship on which the convection model can be constructed. The details of how this model can be constructed are given in Augustson & Mathis (2018). The parameters needed to see how this model can be leveraged to give estimates of the rotational and diffusive influence are

$$\begin{aligned} z^3 &= \frac{k^2}{k_z^2}, \quad q = \frac{N_0}{N}, \quad O = q \sqrt{\frac{3}{2}} \frac{\cos \theta}{5\pi \text{Ro}_c} = qO_0, \\ K &= q \frac{\kappa k_z^2}{N_0} = qK_0, \quad V = q \frac{\nu k_z^2}{N_0} = qV_0, \end{aligned} \quad (1)$$

where k is the magnitude of the wavevector characterizing the mode that maximizes the heat flux, k_z is its vertical component, and θ is the colatitude. Note that the variation of the superadiabaticity for this system is given by $\epsilon = H_P \beta / T$, meaning that $N^2 = g \alpha_T T \epsilon / H_P$, where H_P is the pressure scale height and N_0 is the buoyancy flux of the non-diffusive and nonrotating system provided by the Malkus-Howard convection theory, β is the potential temperature gradient, κ is the thermal diffusion coefficient, ν is the viscous diffusion coefficient. The convective Rossby number is

$$\text{Ro}_c = \frac{v_0}{2\Omega_0 \ell_0} = \frac{\sqrt{6}N_0}{10\pi\Omega_0}, \quad (2)$$

where Ω_0 is the constant angular velocity of the system and use has been made of the fact that the characteristic velocity of the nonrotating system v_0 is derived from the nonrotating and nondiffusive case as $v_0 = s_0/k_0 = \sqrt{6}N_0\ell_0/(5\pi)$, where s_0 is the growth rate derived from the dispersion relationship in the nondiffusive and nonrotating case. Two relevant equations are the dispersion relationship linking the normalized growth rate $\hat{s} = s/N_0$ to q and z , and the heat flux F to be maximized with respect to z

$$\begin{aligned} &(\hat{s} + K_0 q z^3) \left(z^3 (\hat{s} + V_0 q z^3)^2 + 4O_0^2 q^2 \right) \\ &- (z^3 - 1)(\hat{s} + V_0 q z^3) = 0, \end{aligned} \quad (3)$$

$$\frac{F}{F_0} = \frac{1}{q^3} \left[\frac{\hat{s}^3}{z^3} + V_0 q \hat{s}^2 \right]. \quad (4)$$

To assess the scaling of the superadiabaticity, the velocity, and the horizontal wavevector, a further assumption must be made in which the maximum heat flux is invariant to any parameters, namely that $\max[F] = F_0$ so the heat flux is equal to the maximum value F_0 obtained in the Malkus-Howard turbulence model for the nonrotating case. Therefore, building this convection model consists of three steps: deriving a dispersion relationship that links \hat{s} to q and z , maximizing the heat flux with respect to z , and assuming an invariant maximum heat flux that then closes this three variable system.

3 Convection Model

In the case of planetary and stellar interiors, the viscous damping timescale is generally longer than the convective overturning timescale (e.g., $V_0 \ll N_0$). Thus, the maximized heat flux invariance is much simpler to treat. In particular, the flux invariance condition under this assumption is then

$$\begin{aligned} \frac{\max[F]}{F_0} &= \frac{\hat{s}^3}{q^3 z^3} + \frac{V_0 \hat{s}^2}{q^2} \bigg|_{\max} \approx \frac{\hat{s}^3}{q^3 z^3} \bigg|_{\max} = 1 \\ \implies \hat{s} &= qz + \mathcal{O}(V_0/N_0). \end{aligned} \quad (5)$$

One primary assumption of this convection model is that the magnitude of the velocity is defined as the ratio of the maximizing growth rate and wavevector. With the above approximation, the velocity amplitude can be defined generally. The velocity relative to the nondiffusive and nonrotating case scales as

$$\frac{v}{v_0} = \left(\frac{5}{2} \right)^{\frac{1}{6}} \frac{\hat{s}}{q z^{3/2}} = \left(\frac{5}{2} \right)^{\frac{1}{6}} z^{-\frac{1}{2}}. \quad (6)$$

To find the scaling of the heat flux maximizing wavevector $k = z^{3/2}$ and the superadiabaticity $\epsilon/\epsilon_0 = q^{-2}$, one may find the implicit wavevector derivative of the growth rate \hat{s} from Equation 3 and equate it to the derivative of the heat flux $\partial F/\partial z = \hat{s}/z$, which neglects the heat flux arising from the viscous effects. Using the heat-flux invariance, e.g. letting $\hat{s} = qz$, the constraining dispersion relationship (Equation 3) can be manipulated to solve for q as a function of z . Substituting this solution into the equation resulting from the flux maximization yields an equation solely for the wavevector z :

$$\begin{aligned} &z^3 (V_0 z^2 + 1)^2 \times \\ &[3V_0 K_0 z^4 (2z^3 - 3) + z^2 (V_0 + K_0) (4z^3 - 7) + 2z^3 - 5] - \\ &\frac{6 \cos^2 \theta}{25\pi^2 \text{Ro}_c^2} [K_0 (3V_0 z^5 + z^3 + 2) + V_0 (5z^3 - 2) + 3z] = 0. \end{aligned} \quad (7)$$

4 Wave Excitation and Energy Flux

4.1 Gravito-Inertial Waves

Internal gravito-inertial waves (GIWs) are a class of fluid waves where buoyancy and the Coriolis acceleration serve as the restoring forces (e.g., Lee & Saio, 1997; Dintrans & Rieutord, 2000; Ballot *et al.*, 2010; Prat *et al.*, 2016). Within stars and planets with convectively stable regions and potentially convective regions, each class of possible waves have frequency ranges over which they can propagate, permitting nonlocal transport through radiative damping, corotation resonances, as well as through nonlinear wave breaking (e.g., Schatzman, 1993; Mathis *et al.*, 2008; Rogers, 2015; Pinçon *et al.*, 2017). Considering local approximations to these waves, the following can be seen. Pure gravity waves may propagate in stable regions if their frequency (ω) is less than the Brunt-Väisälä frequency, and they are otherwise evanescent. Pure inertial waves may propagate in rigidly-rotating convective regions when their frequency is less than twice the local rotation rate. In convectively stable regions where rotation is important, GIWs may propagate if their frequency falls within the range between ω_- and ω_+ (e.g., Gerkema & Shrira, 2005),

$$\omega_{\pm} = \frac{1}{\sqrt{2}} \sqrt{N_r^2 + f^2 + f_{ss}^2 \pm \sqrt{(N_r^2 + f^2 + f_{ss}^2)^2 - (2N_r f)^2}}, \quad (8)$$

where N_r is the Brunt-Väisälä frequency in the stably stratified region, $f = 2\Omega_0 \cos \theta$, $f_{ss} = 2\Omega_0 \sin \theta \sin \psi$, and ψ is an angle in the plane transverse to the local effective gravity vector. At the pole in a convectively stable region, this implies that the frequency must be between $2\Omega_0$ and N_r for the wave to propagate, where the Brunt-Väisälä frequency is typically much larger than the rotational frequency in the radiative core of late-type stars and the radiative envelope of early-type stars (e.g., Aerts *et al.*, 2010). More generally, at

other latitudes, the hierarchy of extremal propagative wave frequencies satisfy the inequality $\omega_- < 2\Omega_0 < N_r < \omega_+$. As these waves propagate, the Brunt-Väisälä frequency varies, for instance it becomes effectively zero in the convection zone. This implies that waves in the frequency range $\omega < 2\Omega_0$ are classified as sub-inertial GIWs in stable regions, becoming pure inertial waves in convective regions. Waves in the frequency range $\omega \geq 2\Omega_0$ are classified as super-inertial GIWs in the stable region become evanescent in the convective region as pure gravity waves.

4.2 Wave Excitation Mechanisms

One mechanism for exciting waves arises from stochastic motions in the convection zone due to Reynolds stresses interacting with evanescent super-inertial GIWs or propagating inertial and sub-inertial waves as well as directly exciting those waves when the convective flows penetrate into radiative zones. Such excitation mechanisms have been captured in experiments and detected observationally (e.g., Neiner *et al.*, 2012; Aerts & Rogers, 2015; Le Bars *et al.*, 2015). Moreover, the convective excitation of waves and their associated transport processes have been examined extensively both through theoretical modeling (e.g., Press, 1981; Belkacem *et al.*, 2009; Pinçon *et al.*, 2016) and through numerical simulations of convective flows interacting with a stable layer (e.g., Rogers *et al.*, 2013; Alvan *et al.*, 2015; Lecoanet *et al.*, 2015). Turbulence in convective regions is modified by rotation and the rate of downscale energy transfer is reduced. In regimes of rapid rotation (e.g., low convective Rossby number), strongly anisotropic flows develop that result from non-linear interactions of propagative inertial waves (e.g., Davidson, 2013). Such dynamics take place whether or not there is a stably stratified region. However, when a stable zone is present, there are two distinct regimes: one where turbulence weakly influenced by rotation is coupled with evanescent super-inertial GIWs and another where turbulence is strongly influenced by rotation and is thus intrinsically and strongly coupled with sub-inertial GIWs (e.g., Galtier, 2003; Clark di Leoni *et al.*, 2014; Mathis *et al.*, 2014). Nevertheless, these GIW and convection interactions and the transport processes arising from them have not yet been taken into account. However, some steps toward incorporating them into stellar models have already been achieved. For instance, there has been a substantial effort to account for the transport of angular momentum and chemical species by pure gravity waves in pre-main-sequence stars to stars in the penultimate pre-supernovae state (e.g., Talon & Charbonnel, 2008; Charbonnel *et al.*, 2013; Fuller & Ro, 2018).

4.3 Interfacial Gravito-Inertial Wave Flux Estimates

There are many models for estimating the magnitude of the gravity wave energy flux arising from the waves excited by convective flows. One of the first and most straightforward of such estimates is described in Press (1981), where the wave flux across an interface connecting a convective region to a stable zone is computed by matching their respective pressure perturbations at that interface. Because the wave excitation occurs at an interface, the pressure perturbations are more important than the Reynolds stresses of the flows. What is more, the model assumes that the convective source is a delta function in space and time. So, the model permits only a single horizontal spatial scale $2\pi/k_c$ and a single time scale for the convection $2\pi/\omega_c$ that also selects the depth of the transitional interface where $N(r) = \omega_c$ for gravity waves, where $\omega_c = \omega_0/\sqrt{z}$ with $\omega_0 = 2\pi v_0/\ell_0$, which lends itself well to the above convection model. This approach yields a wave flux proportional to the product of the convective

kinetic energy flux and the ratio of the wave frequency to the Brunt-Väisälä frequency in the case of gravity waves.

The convective model established above captures some aspects of the influence of rotation on the convective flows. Therefore, the impact of the Coriolis force on the stochastic excitation of GIWs can be evaluated. In this context, recent work has established an estimate of the GIW flux (André *et al.*, 2017). It can be used to estimate the rotational scaling of the amplitude of the wave flux arising from the modified properties of the convective driving. In André *et al.* (2017), the vertical GIW energy flux is computed from the horizontal average of the product of the vertical velocity and pressure perturbation that, given the linearization of the Boussinesq equations for monochromatic waves propagating in a selected horizontal direction, can be evaluated to be

$$F_z = \frac{1}{2} \rho_0 \frac{\omega^2 - f^2}{\omega k_{\perp}^2} k_z v_w^2, \quad (9)$$

where v_w is the magnitude of the vertical velocity of the wave.

Following Press (1981), further assumptions are necessary to complete the estimate of the wave flux. The convection is turbulent. So the fluctuating part of the velocity field is of the same order of magnitude as the convective eddy turnover velocity $v_c \approx \omega_c/k_c$, which implies that convective pressure perturbations are approximately $P_c = \rho_0 v_c^2$. Assuming that the pressure is continuous across the interface between the convectively stable and unstable regions, the horizontally-averaged pressure perturbations of the propagating waves excited at the interface must then be equal to the turbulent pressure on the convective side of the interface. Those pressure perturbations follow from the solution for the vertical velocity and the nondiffusive Boussinesq equations. Flows in a gravitationally stratified convective medium tend to have an extent in the direction of gravity that is much larger than their extent in the transverse directions. Therefore, the horizontal wavenumber of the convective flows is much greater than the vertical wavenumber. Within the context of the single-mode convection model derived above, this implies that $k_{\perp,c} \approx \omega_c/v_c$. For efficient wave excitation, the frequency of the wave needs to be close to the source frequency (Press, 1981; Lecoanet & Quataert, 2013), which means that the horizontal scale of the waves will be similar to that of the convection. Therefore, the spectral density in frequency space of the wave energy flux is approximately

$$F_z \approx \frac{1}{2} \rho_0 v_c^3 \omega^2 \frac{[\omega^2 f_{ss}^2 + (N_r^2 - \omega^2)(\omega^2 - f^2)]^{\frac{1}{2}}}{\omega^2 f_s^2 + (N_r^2 - \omega^2)(\omega^2 - f^2)}. \quad (10)$$

Finally, taking the ratio of the rotation-influenced flux to the flux in the nonrotating case to better isolate the changes induced by rotation, assuming that the Brunt-Väisälä frequency is not directly impacted by rotation, and at a fixed wave frequency ω , one has that

$$\frac{F_z}{F_0} \approx \left(\frac{v}{v_0} \right)^3 \omega \frac{\{ (N_r^2 - \omega^2) [\omega^2 f_{ss}^2 + (N_r^2 - \omega^2)(\omega^2 - f^2)] \}^{\frac{1}{2}}}{\omega^2 f_s^2 + (N_r^2 - \omega^2)(\omega^2 - f^2)}, \quad (11)$$

with $f_s = 2\Omega_0 \sin \theta$ and f_{ss} defined as above. To make this a bit more parametrically tractable, one can normalize the wave frequency as $\sigma = \omega/N_r$, and cast the rotational terms into a product of the stiffness of the transition $S = N_r/N_0$, with the convective Rossby number as defined above in §2 with Equations 1 and 2. Doing so yields

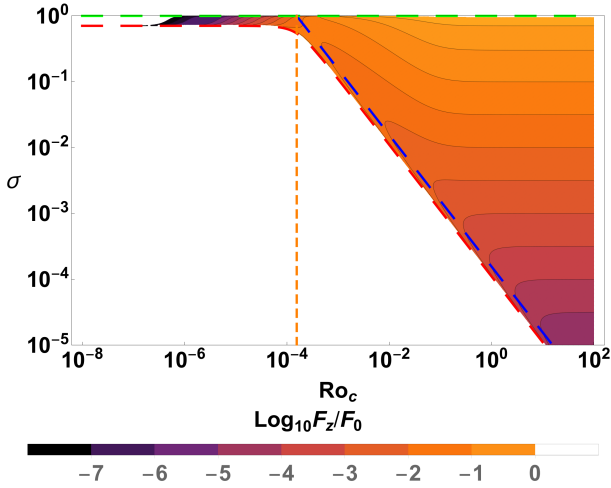


Figure 1: Convective Rossby number dependence of the ratio of the interfacial gravity wave flux excited by rotating convection relative to the nonrotating case F_z/F_0 for the non-diffusive convection model at $\theta = \pi/4$, with an interface stiffness of $S = 10^3$ and a horizontal direction of $\psi = \pi/2$. The red dashed line indicates the lower frequency cutoff σ_- , the green dashed line indicates the upper cutoff frequency of $\sigma = 1$ since the wave flux is being compared to a non-rotating case, whereas the blue dashed line indicates a wave Rossby number of $\widetilde{Ro}_w = 1$. The vertical dashed orange line indicates the critical convective Rossby number.

$$\frac{F_z}{F_0} \approx \left(\frac{v}{v_0}\right)^3 \left[Ro_w^{-2} \sin^2 \theta + (\sigma^{-2} - 1)(1 - Ro_w^{-2} \cos^2 \theta) \right]^{-1} \left[(\sigma^{-2} - 1) Ro_w^{-2} \sin^2 \theta \sin^2 \psi + (\sigma^{-2} - 1)^2 (1 - Ro_w^{-2} \cos^2 \theta) \right]^{\frac{1}{2}}, \quad (12)$$

where $Ro_w = \omega/2\Omega_0 = 5\pi\sigma Ro_c S/\sqrt{6}$ and the wave Rossby number is $\widetilde{Ro}_w = Ro_w/\sqrt{\sin^2 \theta \sin^2 \psi + \cos^2 \theta}$.

This is depicted in Figure 1, where the colored region exhibits the magnitude of the logarithm of the flux ratio. An interfacial stiffness of $S = 10^3$ is chosen as it is a rough estimate of the potential stiffness in most stars, being the ratio of the buoyancy time-scale in the stable region to the convective overturning time. The choice of latitude determines the width of the frequency band of sub-inertial waves, where it is a minimum at the pole and maximum near the equator, with $\theta = \pi/4$ here and $\theta \approx \pi/2$ shown in Augustson & Mathis (2018). The direction of $\psi = \{-\pi/2, \pi/2\}$ is chosen as it represents the maximum value of the flux ratio for the choice of other parameters and represents the waves travelling toward either of the poles as the flux ratio is an even parity function of the horizontal direction. Specifically, the poleward wave flux ratio is greater than the other extremal choice of the prograde or retrograde wave flux ratios. In particular, given the range of ω_{\pm} , there are no sub-inertial waves in the prograde or retrograde propagation case ($\psi = \{0, \pi\}$, respectively), whereas the super-inertial waves may still propagate with roughly the same frequency range. The white region corresponds to the domain of evanescent waves for a

given Rossby number with frequencies below the lower cut-off frequency (σ_- , dashed red line) for propagating GIWs. At frequencies above this threshold there is a frequency dependence of the flux ratio until reaching the upper cut-off where $\sigma = \omega/N_r = 1$, which arises due to the domain of validity when comparing GIW to gravity wave fluxes. Indeed, gravity waves may propagate if $\omega < N_r$, whereas super-inertial GIWs may propagate even when $N_r < \omega < \omega_+$. The transition between super-inertial and sub-inertial waves is demarked with the dashed green line, with super-inertial waves for $\widetilde{Ro}_w > 1$ and sub-inertial waves for $\widetilde{Ro}_w < 1$. Here, interfacially-excited super-inertial waves exhibit both a frequency and convective Rossby number dependence. Specifically, the wave flux decreases algebraically with frequency at a fixed convective Rossby number and have a reduced flux for convective Rossby numbers below unity. The interfacially-excited sub-inertial waves possess a small frequency domain at a fixed convective Rossby number over which they are propagative. The sub-inertial wave flux increases with decreasing convective Rossby number until a critical convective Rossby number $Ro_{c,crit} = \sqrt{6}/(5\pi S)$ as depicted by the vertical dashed orange line in Figure 1. Below this critical convective Rossby number, the sub-inertial wave flux decreases and their frequency domain is further restricted until it vanishes entirely and there are no propagative super-inertial waves. The effect of the stiffness is to lower (raise) the value of the critical convective Rossby number for larger (smaller) values of S , which corresponds to the ratio of the buoyancy time-scale in the radiative zone to the convective overturning time. This may have important consequences for the wave-induced transport of angular momentum during the evolution of rotating stars. In particular, the convective Rossby number can vary by several orders of magnitude over a star's evolution from the PMS to its ultimate demise. Moreover, it can vary internally as a function of radius due to the local amplitude of the convective velocity and due to transport processes, angular momentum loss through winds, and structural changes that modify the local rotation rate (e.g., Landin *et al.*, 2010; Mathis *et al.*, 2016; Charbonnel *et al.*, 2017).

4.4 Reynolds Stress Contributions to GIW Amplitudes

So far, the wave excitation mechanism has been considered to be interfacial, as in Press (1981). Yet this estimate omits wave flux linked to their excitation by convective Reynolds stresses (e.g., Belkacem *et al.*, 2009; Samadi *et al.*, 2010; Lecoanet *et al.*, 2015). The amplitude and the wave flux of the GIWs may be estimated using the results of Mathis *et al.* (2014), where the impact of rotation on the waves is treated coherently. In a means similar to Goldreich & Kumar (1990) and Lecoanet & Quataert (2013), although with a greater degree of computational complexity, one may derive the wave amplitudes for GIWs in a f-plane. One must first find solutions to the homogeneous Poincaré equation for the GIWs and then use linear combinations of those solutions to construct solutions to the forced Poincaré equation as in Appendix B of Gerkema & Shrira (2005) and Equation 27 of Mathis *et al.* (2014). Those solutions can then be employed to construct asymptotic expressions for the wave amplitude for a given forcing function in the convection zone as in Equations 28 and 29 of Mathis *et al.* (2014). This can be evaluated analytically using the properties of the Fourier transform, the convolution theorem, and the properties of Dirac delta functions (see Augustson & Mathis (2018) for details).

Precisely defining the spectral properties of the Reynolds stresses in rotating thermal convection is a difficult task. The

symmetries of homogeneous and isotropic stirred turbulence do not generally exist in these systems. Thus, for simplicity and as a first approximation, the turbulence model presented in Lecoanet & Quataert (2013) is adopted here. In this model, the convection is treated as a Kolmogorov-Heisenberg spectrum of eddies, with the eddies spanning the size spectrum from a maximum cut off size of H to eddies of size $h < H$ and with a large-scale turnover frequency of ω_c and eddy time-scale with $\omega_e > \omega_c$. The eddy velocity thus scales as $u_h = u_c(h/H)^{1/3} = u_c(\omega_e/\omega_c)^{-1/2}$, where $\omega_e = u_h/h$ and u_c is the rms convective velocity. Thus, the Reynolds stresses due to a single eddy are considered to be $\widehat{v_i v_j} \propto h^3 u_h^2$. Given this prescription of convection, one may estimate the magnitude of the forcing function due to the convective Reynolds stresses in the forced Poincaré equation that describes the wave motion. Specifically, the amplitude of the waves may be estimated, which leads to subsequent scaling relationships for the spectral density $\partial^2 P / \partial \ln \omega \partial \ln k_\perp$ of the wave flux that has been integrated in horizontal wavevector k_\perp . These scaling relationships for the gravity wave flux have shown to hold up well in numerical simulations (e.g., Couston *et al.*, 2018). With a turbulence model in hand, one may closely follow Lecoanet & Quataert (2013) with some new assumptions about the mode number density to find the scaling for the wave flux ratio, where it is left to the reader to seek out the details of the derivation in Augustson & Mathis (2018). Note that again $S = N_r/N_0$ and $\omega_c^2 = 6v^2 N_0^2 / (25\pi^2 v_0^2)$. Thus, following the approach in the interfacial excitation case for nondimensionalizing the Reynolds stress driven flux ratio estimate, one has that

$$\begin{aligned} \frac{F_{z,j}}{F_0} &= \frac{n_z \int dk_\perp d_j G_j^2}{n_0 p^2 \int dk_\perp d_j G_j^2|_0} \left(\frac{v}{v_0} \right)^{\frac{9}{2}} (1 - \text{Ro}_w^{-2} \cos^2 \theta)^3 \\ &\times ([\ell_s L^{-1} - 6\ell_0 L^{-1} / (25\pi^2 S^2)] \sigma^{-2} - 1) \\ &\times \{ [\ell_s L^{-1} - 6\ell_0 L^{-1} / (25\pi^2 S^2)] (1 - \text{Ro}_w^{-2} \cos^2 \theta) \sigma^{-2} \\ &+ \widetilde{\text{Ro}}_w^{-2} - 1 \}^{-1}, \end{aligned} \quad (13)$$

where $\text{Ro}_w = \omega / 2\Omega_0 = \sqrt{25/6\pi} \text{Ro}_c S \sigma$ and j = sub or sup for sub-inertial and super-inertial waves respectively, and $p = \sqrt{1 - \widetilde{\text{Ro}}_w^{-2} / (1 - \text{Ro}_w^{-2} \cos^2 \theta)}$. The ratio of the mode number densities is

$$\begin{aligned} \frac{n_z}{n_0} &= \left[\ell_s L^{-1} \left| \frac{\sigma^{-2} - 1}{1 - \text{Ro}_w^{-2} \cos^2 \theta} + \frac{\delta^2 \text{Ro}_w^{-2}}{\cos^2 \theta} \right|^{\frac{1}{2}} \right. \\ &\quad \left. + \ell_0 L^{-1} \left| \frac{\delta^2 \text{Ro}_w^{-2}}{\cos^2 \theta} - \frac{6v^2 \sigma^{-2} / (25\pi^2 v_0^2 S^2) + 1}{1 - \text{Ro}_w^{-2} \cos^2 \theta} \right|^{\frac{1}{2}} \right] \\ &\times \left[\ell_s L^{-1} (\sigma^{-2} - 1)^{\frac{1}{2}} + \ell_0 L^{-1} (6\sigma^{-2} / (25\pi^2 S^2) + 1)^{\frac{1}{2}} \right]^{-1}, \end{aligned} \quad (14)$$

where the horizontal phase shift is $\delta = \sin \theta \cos \theta \sin \psi / (1 - \text{Ro}_w^{-2} \cos^2 \theta)$. The Fourier transforms and convolutional integrals of the asymptotic eigenfunctions for the GIWs and the convective source function result in an integral of the wave-turbulence interaction structure functions $n_z d_j G_j$ with respect to the horizontal wave number. These functions are composed of a

mode excitation depth d_j , a wave structure function G_j , and a mode number density n_z . For the super-inertial waves, this is

$$\begin{aligned} Q_{\text{sup}} &= \int_{2\pi L^{-1}}^{k_\perp} dk'_\perp d_{\text{sup}} G_{\text{sup}}^2 \\ &= [p^2 (2\delta + \zeta)^2 + (1 + p^2 - \delta^2 - \delta\zeta)] \times \\ &\quad \int_{2\pi L^{-1}}^{k_\perp} dk'_\perp \ell_0 e^{-k'_\perp (p\ell_0 + 2\Delta)} \\ &= [p^2 (2\delta + \zeta)^2 + (1 + p^2 - \delta^2 - \delta\zeta)] [\ell_s \ell_0^{-1} \Delta + p]^{-1} \times \\ &\quad [e^{-2\pi L^{-1} (\ell_s \Delta + p\ell_0)} - e^{-k_\perp (\ell_s \Delta + p\ell_0)}]. \end{aligned} \quad (15)$$

For the sub-inertial waves, this is

$$\begin{aligned} Q_{\text{sub}} &= \int_{2\pi L^{-1}}^{k_\perp} dk'_\perp d_{\text{sub}} G_{\text{sub}}^2 = \int_{2\pi L^{-1}}^{k_\perp} dk'_\perp \ell_0 \times \\ &\quad [p^2 (2\delta + \zeta)^2 \cos^2(k_\perp \ell_s \Delta) + (\delta^2 + \delta\zeta + p^2 - 1)^2 \sin^2(k_\perp \ell_s \Delta)] \\ &= \frac{(k_\perp L - 2\pi)}{2\ell_0^{-1} L} [p^2 (2\delta + \zeta)^2 + (\delta^2 + \delta\zeta + p^2 - 1)^2] + \\ &\quad [p^2 (2\delta + \zeta)^2 - (\delta^2 + \delta\zeta + p^2 - 1)^2] \times \\ &\quad \frac{\sin[2k_\perp \ell_s \Delta] - \sin[4\pi \ell_s L^{-1} \Delta]}{4\ell_s \ell_0^{-1} \Delta}, \end{aligned} \quad (16)$$

where $\ell_0 = z_2 - z_c$, $\ell_s = z_c - z_1$, $L = z_2 - z_1$, are the depths of the convection zone, stable layer, and whole domain respectively, with z_c being the point of sharp variation in the Brunt-Väisälä frequency modelled here using an Heaviside distribution. Here ζ is an anisotropy parameter for the convective Reynolds stresses, with $\zeta = 1$ for isotropic flows, and

$$\Delta = \ell_s \left| \frac{\sigma^{-2} - 1}{1 - \text{Ro}_w^{-2} \cos^2 \theta} + \frac{\delta^2 \text{Ro}_w^{-2}}{\cos^2 \theta} \right|^{\frac{1}{2}}, \quad (17)$$

is the effective wave cavity size for a given frequency.

Figure 2 separately shows the flux ratio of convectively-excited GIWs relative to gravity waves in a nonrotating limit and omitting the factor of $Q_j / Q_j|_0$, denoted as $\mathcal{Z} / \mathcal{Z}_0$, as well as the flux ratios that include this prefactor for the super-inertial and sub-inertial waves. The parameters are chosen to be the same as for the interfacial case (Figure 1), with the additional choice of a symmetric domain and assuming isotropic turbulence so that $\zeta = 1$. Note that the effect of $\zeta > 1$ is to lower the GIW flux relative to the nonrotating case. In Figure 2(a), two distinct regions appear to the left and to the right of the $\widetilde{\text{Ro}}_w = 1$ line, which is drawn in blue. Waves to the right of this line have $\widetilde{\text{Ro}}_w > 1$ and thus correspond to super-inertial waves, and those on the left correspond to sub-inertial waves. The dashed red line is the lower cutoff frequency for propagative GIWs. Again there is the critical convective Rossby number, depicted by the vertical dashed orange line, below which there are no super-inertial waves and only a small frequency band of sub-inertial waves are permitted. From Figures 2(a) and (b), it is

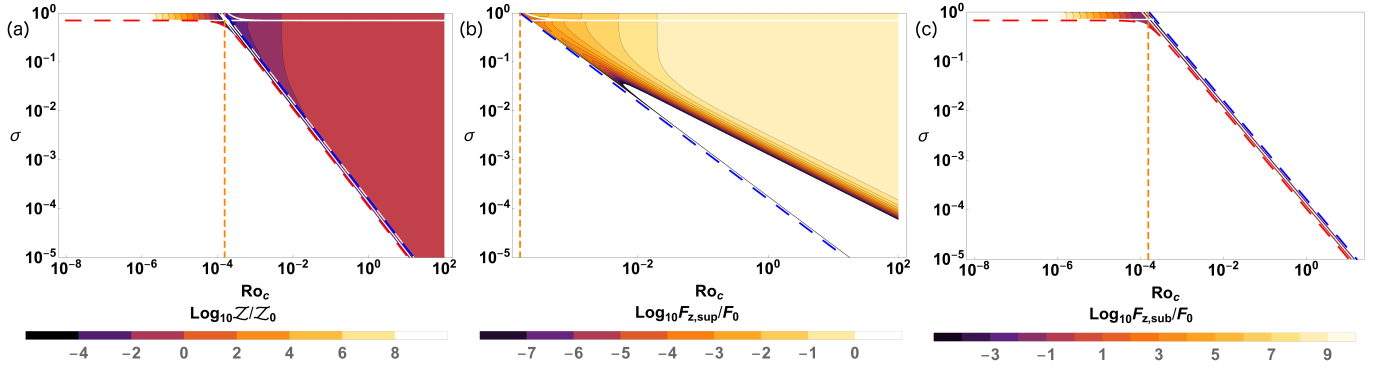


Figure 2: Convective Rossby number dependence of the ratio of the GIW flux excited by rotating convection relative to the nonrotating case F_z/F_0 for the nondiffusive convection model at $\theta = \pi/4$, with an interface stiffness of $S = 10^3$, a horizontal direction of $\psi = \pi/2$, in a symmetric domain where $\ell_s = \ell_0 = L/2$, and with $\zeta = 1$. (a) The flux Z/Z_0 is shown without the influence of the Q_j , which serves to highlight its inclusion in the next two panels. In all panels, the dashed red line denotes the lower wave frequency cutoff σ_- , whereas the dashed blue line corresponds to $\widetilde{Ro}_w = 1$. The vertical dashed orange line indicates the critical convective Rossby number. The upper cutoff is $\sigma = 1$ as this is the maximum frequency for which the rotating and non-rotating cases can be compared. (b) The total wave flux $F_{z,sup}/F_0$ for the super-inertial waves, illustrating the truncation of the frequency spectrum due to Q_{sup} . (c) The total wave flux $F_{z,sub}/F_0$ for the sub-inertial waves, exhibiting the increasing flux enhancement when σ is such that $\widetilde{Ro}_w \approx 1$ and $Ro_c < Ro_{c,crit}$.

clear that the flux ratio decreases for super-inertial waves as the convective Rossby number decreases, just as in the interfacial excitation model discussed above and shown in Figure 1. Moreover, this also indicates that the frequency range of the GIWs remains restricted at lower Rossby numbers when comparing to the interfacially-excited GIWs. Indeed, the convectively-excited super-inertial waves have a more restricted frequency range due to the exponential behavior of the Q_{sup} factor when compared to the interfacially-excited waves. Particularly, the flux ratio drops below the lower cutoff value of 10^{-8} and becomes vanishingly small in the white region between the dark lower bound and the dashed blue line. The convectively-excited sub-inertial GIW flux ratio is shown in Figure 2(c), where it is evident that the waves remain highly restricted to a narrow frequency band as is the case for the interfacially-excited sub-inertial waves. However, when the convective Rossby number is below the critical convective Rossby number, the convectively-excited sub-inertial waves have an exponentially increasing flux ratio with decreasing Rossby number. For sub-inertial waves propagating in regions where the convective Rossby number is greater than that critical value, there is a very narrow band of frequencies close to $\sigma = \sigma_-$ for which the flux ratio is very large in an apparent resonance. Given the form of Q_{sub} , this is expected due to the inverse dependence of Q_{sub} on Δ . The super-inertial waves, on the other hand, have $Q_{sup} \propto (\Delta + p)^{-1}$ and so do not have the same peaked feature. When further comparing the interfacially-excited and the convectively-excited GIWs, it appears that there is a transition in frequency below which the convectively-excited super-inertial waves will have a greater flux ratio than the interfacially excited ones. The sub-inertial waves, on the other hand, have a much richer suite of behavior, with there being a transition in convective Rossby number where a similar exchange between the dominant excitation mechanism occurs. There is also a broader range of frequencies where the interfacially-excited sub-inertial waves have an appreciable flux ratio, and yet a very strong resonant peak for the convectively-excited waves that dwarfs the magnitude of the flux ratio of interfacially-excited waves. Such resonances are not without precedence, as they appear in numerical simula-

tions (Rogers *et al.*, 2013) and may be at the origin of stochastically excited sub-inertial waves observed for some rapidly rotating stars Neiner *et al.* (2012).

5 Summary and Discussion

A simple model of rotating convection originating with Stevenson (1979) has been extended to include thermal and viscous diffusion for any convective Rossby number. Moreover, a systematic means of developing such models for an arbitrary dispersion relation have also been shown. An explicit expression is given for the scaling of the horizontal wavenumber in terms of the Rossby number and diffusion coefficients under the constraint that the values of the diffusive time scale are less than the convective time scale (Equation 7). The scaling of the velocity in terms of that wavenumber is also given. As shown in Augustson & Mathis (2018), these match the expressions given in Stevenson (1979), as well as the numerical results found in the 3D simulations of Käpylä *et al.* (2005) and Barker *et al.* (2014) asymptotically at low Rossby number and without diffusion.

As a first step in examining the impact of rotation on the stochastic excitation of GIWs, the convection model is applied to the interfacial wave excitation paradigm developed in Press (1981). Following the wave dynamics given in Mathis *et al.* (2014) and André *et al.* (2017), one can derive that the Press (1981) model implies that the wave flux for propagative waves should decrease asymptotically as $Ro_c^{3/5}$. Also, for a given stiffness of the transition between the radiative zone and the convection zone, the domain of allowed frequencies for propagative waves steadily decreases as seen in Figure 1. To better assess the influence of the convective Reynolds stresses and of rotation on the GIWs, a third wave flux estimate is constructed using an explicit computation of the amplitude for both the super-inertial and sub-inertial waves derived in Mathis *et al.* (2014). The convection model of Lecoanet & Quataert (2013) is then invoked as means of estimating the Reynolds stresses and their variation with rotation. It is found again that the wave flux decreases with Rossby number (Figure 2) due to the influence of the convective velocities. These fluxes also depend upon

the horizontal wave number of the wave. More strikingly, however, the super-inertial waves additionally have a truncated frequency spectrum of waves capable of transporting energy whereas the sub-inertial waves have a small range of frequencies centered around $\omega_0 \propto N_r Ro_c^{-1}$ over which their flux is greatly increased to levels similar to the nonrotating cases. In stark contrast to the interfacially excited waves, the convectively-excited sub-inertial waves also exhibit an exponentially increasing wave flux relative to the nonrotating case below a critical convective Rossby number. This may have substantial consequences for the transport and mixing of angular momentum, chemical species, and heat in rotating stellar and planetary interiors.

Acknowledgments

K. C. Augustson and S. Mathis acknowledge support from the ERC SPIRE 647383 grant and PLATO CNES grant at CEA/DAP-AIM.

References

- Aerts, C., Christensen-Dalsgaard, J., & Kurtz, D. W. 2010, *Asteroseismology*.
- Aerts, C. & Rogers, T. M. 2015, *ApJ*, 806, L33.
- Aerts, C., Van Reeth, T., & Tkachenko, A. 2017, *ApJ*, 847, L7.
- Alvan, L., Mathis, S., & Decressin, T. 2013, *A&A*, 553, A86.
- Alvan, L., Strugarek, A., Brun, A. S., Mathis, S., & Garcia, R. A. 2015, *A&A*, 581, A112.
- André, Q., Barker, A. J., & Mathis, S. 2017, *A&A*, 605, A117.
- Augustson, K. C. & Mathis, S. 2018, *ApJ*, 869, 33.
- Ballot, J., Lignières, F., Reese, D. R., & Rieutord, M. 2010, *A&A*, 518, A30.
- Barker, A. J., Dempsey, A. M., & Lithwick, Y. 2014, *ApJ*, 791, 13.
- Belkacem, K., Mathis, S., Goupil, M. J., & Samadi, R. 2009, *A&A*, 508, 345.
- Brun, A. S. & Toomre, J. 2002, *ApJ*, 570, 865.
- Chandrasekhar, S. 1961, *Hydrodynamic and hydromagnetic stability*.
- Charbonnel, C., Decressin, T., Amard, L., Palacios, A., & Talon, S. 2013, *A&A*, 554, A40.
- Charbonnel, C., Decressin, T., Lagarde, N., Gallet, F., Palacios, A., *et al.* 2017, *A&A*, 605, A102.
- Clark di Leoni, P., Cobelli, P. J., Mininni, P. D., Dmitruk, P., & Matthaeus, W. H. 2014, *Physics of Fluids*, 26, 035106.
- Couston, L.-A., Lecoanet, D., Favier, B., & Le Bars, M. 2018, *Journal of Fluid Mechanics*, 854, R3.
- Davidson, P. 2013, *Turbulence in Rotating, Stratified and Electrically Conducting Fluids* (Cambridge University Press). ISBN 9781107434349.
- Dintrans, B. & Rieutord, M. 2000, *A&A*, 354, 86.
- Dintrans, B., Rieutord, M., & Valdettaro, L. 1999, *Journal of Fluid Mechanics*, 398, 271.
- Fuller, J., Cantiello, M., Stello, D., García, R. A., & Bildsten, L. 2015, *Science*, 350, 423.
- Fuller, J. & Ro, S. 2018, *MNRAS*, 476, 1853.
- Galtier, S. 2003, *PhRvE*, 68, 015301.
- Garaud, P. 2018, *Annual Review of Fluid Mechanics*, 50, 275.
- García, R. A., Turck-Chièze, S., Jiménez-Reyes, S. J., Ballot, J., Pallé, P. L., *et al.* 2007, *Science*, 316, 1591.
- Gerke, T. & Shrira, V. I. 2005, *Journal of Fluid Mechanics*, 529, 195.
- Glatzmaier, G. A. & Gilman, P. A. 1982, *ApJ*, 256, 316.
- Goldreich, P. & Kumar, P. 1990, *ApJ*, 363, 694.
- Howard, L. N. 1963, *Journal of Fluid Mechanics*, 17, 405.
- Jouve, L. & Ogilvie, G. I. 2014, *Journal of Fluid Mechanics*, 745, 223.
- Käpylä, P. J., Korpi, M. J., Stix, M., & Tuominen, I. 2005, *A&A*, 438, 403.
- Kichatinov, L. L. 1986, *Geophysical and Astrophysical Fluid Dynamics*, 35, 93.
- Kumar, P., Talon, S., & Zahn, J.-P. 1999, *ApJ*, 520, 859.
- Kupka, F. & Muthsam, H. J. 2017, *Living Reviews in Computational Astrophysics*, 3, 1.
- Landin, N. R., Mendes, L. T. S., & Vaz, L. P. R. 2010, *A&A*, 510, A46.
- Le Bars, M., Lecoanet, D., Perrard, S., Ribeiro, A., Rodet, L., *et al.* 2015, *Fluid Dynamics Research*, 47, 045502.
- Lecoanet, D., Le Bars, M., Burns, K. J., Vasil, G. M., Brown, B. P., *et al.* 2015, *PhRvE*, 91, 063016.
- Lecoanet, D. & Quataert, E. 2013, *MNRAS*, 430, 2363.
- Lecoanet, D., Vasil, G. M., Fuller, J., Cantiello, M., & Burns, K. J. 2017, *MNRAS*, 466, 2181.
- Lee, U. & Saio, H. 1997, *ApJ*, 491, 839.
- Malkus, W. V. R. 1954, *Proceedings of the Royal Society of London Series A*, 225, 196.
- Mathis, S. 2009, *A&A*, 506, 811.
- Mathis, S. 2013, In *Lecture Notes in Physics, Berlin Springer Verlag*, edited by M. Goupil, K. Belkacem, C. Neiner, F. Lignières, & J. J. Green, *Lecture Notes in Physics, Berlin Springer Verlag*, vol. 865, p. 23.
- Mathis, S., Auclair-Desrotour, P., Guenel, M., Gallet, F., & Le Poncin-Lafitte, C. 2016, *A&A*, 592, A33.
- Mathis, S., Neiner, C., & Tran Minh, N. 2014, *A&A*, 565, A47.
- Mathis, S., Talon, S., Pantillon, F.-P., & Zahn, J.-P. 2008, *SoPh*, 251, 101.
- Miesch, M. S. & Toomre, J. 2009, *Annual Review of Fluid Mechanics*, 41, 317.
- Neiner, C., Mathis, S., Saio, H., Lovekin, C., Eggenberger, P., *et al.* 2012, *A&A*, 539, A90.
- Pinçon, C., Belkacem, K., & Goupil, M. J. 2016, *A&A*, 588, A122.
- Pinçon, C., Belkacem, K., & Goupil, M.-J. 2017, In *European Physical Journal Web of Conferences, European Physical Journal Web of Conferences*, vol. 160, p. 02002.
- Prat, V., Lignières, F., & Ballot, J. 2016, *A&A*, 587, A110.
- Press, W. H. 1981, *ApJ*, 245, 286.
- Rogers, T. M. 2015, *ApJ*, 815, L30.
- Rogers, T. M., Lin, D. N. C., McElwaine, J. N., & Lau, H. H. B. 2013, *ApJ*, 772, 21.
- Rogers, T. M. & McElwaine, J. N. 2017, *ApJ*, 848, L1.
- Saio, H., Kurtz, D. W., Takata, M., Shibahashi, H., Murphy, S. J., *et al.* 2015, *MNRAS*, 447, 3264.
- Samadi, R., Belkacem, K., Goupil, M. J., Dupret, M.-A., Brun, A. S., *et al.* 2010, *Ap&SS*, 328, 253.
- Schatzman, E. 1993, *A&A*, 279, 431.
- Stello, D., Cantiello, M., Fuller, J., Huber, D., García, R. A., *et al.* 2016, *Nature*, 529, 364.
- Stevenson, D. J. 1979, *Geophysical and Astrophysical Fluid Dynamics*, 12, 139.
- Talon, S. & Charbonnel, C. 2005, *A&A*, 440, 981.
- Talon, S. & Charbonnel, C. 2008, *A&A*, 482, 597.
- Zahn, J.-P., Talon, S., & Matias, J. 1997, *A&A*, 322, 320.